Frontiers of Physics
https://doi.org/10.1007/s11467-019-0902-7
Front. Phys.
14(4), 43603 (2019)

RESEARCH ARTICLE

Effective models for nearly ideal Dirac semimetals

Feng Tang, Xiangang Wan[†]

National Laboratory of Solid State Microstructures and School of Physics, Nanjing University, Nanjing 210093, China
Collaborative Innovation Center of Advanced Microstructures, Nanjing University, Nanjing 210093, China
Corresponding author. E-mail: [†]*xgwan@nju.edu.cn*
Received April 23, 2019; accepted April 26, 2019

Topological materials (TMs) have gained intensive attention due to their novel behaviors compared with topologically trivial materials. Among various TMs, Dirac semimetal (DSM) has been studied extensively. Although several DSMs have been proposed and verified experimentally, the suitable DSM for realistic applications is still lacking. Thus finding ideal DSMs and providing detailed analyses to them are of both fundamental and technological importance. Here, we sort out 8 (nearly) ideal DSMs from thousands of topological semimetals in *Nature* 566(7745), 486 (2019). We show the concrete positions of the Dirac points in the Brillouin zone for these materials and clarify the symmetry-protection mechanism for these Dirac points as well as their low-energy effective models. Our results provide a useful starting point for future study such as topological phase transition under strain and transport study based on these effective models. These DSMs with high mobilities are expected to be applied in fabrication of functional electronic devices.

Keywords Dirac semimetal, symmetry, effective model

1 Introduction

Since the concept of band topology was introduced in the understanding of quantum Hall effect in two-dimensional (2D) free electron gas (FEG) [1, 2], topological materials (TMs) have remained to be a hot research area in condensed matter physics. Many topological phases have been proposed and especially in the past decade when many TMs were theoretically proposed and some of them were even experimentally confirmed [3–6].

Rather than in the case of quantum Hall insulator in 2D FEG where high magnetic field is necessary [1, 2], time-reversal symmetric materials (namely non-magnetic materials) can also host nontrivial band topology, such as topological insulators protected by time reversal ($\mathcal{T}$) symmetry [3, 4]. Moreover other than time-reversal symmetry, additional spatial symmetry may also protect topological crystalline insulators and semimetals [5–7]. For Dirac semimetals (DSMs) [7–10], the bulk low-energy Hamiltonian around the four-fold degenerate band crossing point (also called Dirac point, DP) can mimic the massless $(3+1)$-D Dirac Hamiltonian. Such a new quantum state attracted extensive research interest [8–13] due to its novel physical consequences such as Klein tunelling [14]. Furthermore, considering lower symmetries in solids rather than Lorentz symmetry, people also proposed type-II DSM with oblique Dirac cones and realized it in $PdTe_2$ and $PtTe_2$ [15–17]. Note that the DPs in these type-II DSMs are relatively far away from the Fermi level (around 1 eV below the Fermi level) [15–17]. Note that two early DSMs, Na_3Bi and Cd_3As_2, both own perfect Fermi surfaces (only containing discrete Dirac points), but they have intrinsic problems hindering their realistic applications: Na_3Bi [9] is not stable in the air while Cd_3As_2 [10] is highly toxic. Since then, there have been many works on discovering DSMs [18–25].

Recently, large-scale database searches for 3D non-magnetic TMs have been done where many TMs were predicted [26–28], which include materials with symmetry protected band crossings near the Fermi level. These TMs databases provide a narrowed-down version of material database for future studies on topological properties. However, it is worth mentioning that further theoretical analyses and calculations may still be necessary before future experimental studies on them: For topological semimetals, one need to further check the positions of the band crossings and their symmetry protection mechanisms as well as their low energy $\boldsymbol{k}\cdot\boldsymbol{p}$ Hamiltonian, key to next-step studies. In this work we focus on the Dirac semimetals (DSMs) and sort out eight (nearly) ideal DSMs. In these DSMs, several are promising since they seem to be quite stable and also non-toxic. We also give detailed analyses of them. These materials provide a fruitful platform to study chiral anomaly [29] and also are expected to be used in fabrications of devices with ultrahigh mobilities [30] in future.

*Special Topic: Recent Advances in Topological Materials (Eds. Yugui Yao, Xiangang Wan, Shengyuan A. Yang & Hua Chen).

Table 1 The selected nearly ideal DSMs out of the TM database [28].

Space groups	63	139	166	167	176	194	223	224
Materials	$K_3Pt_2O_4$	Al_3Nb	$NaZn_4As_3$	Cs_8Ga_{11}	$AgHf_3Cd_3F_{20}$	Na_2MgSn	Pd_3SrO_4	Ag_2O
Dirac points	Z, T, R	Γ–Z	Γ–Z	L, Z	A, L	Γ–A	Γ–X	Γ–X

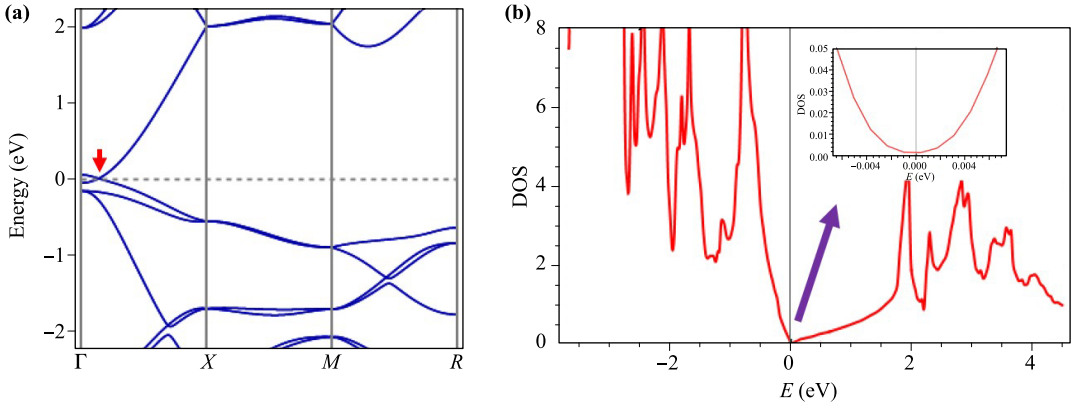

Fig. 1 **(a)** The electronic band structure for Ag_2O ($\mathcal{SG}224$) and the red arrow indicates one DP lying in the high symmetry line Γ–X. **(b)** The density of states for Ag_2O ($\mathcal{SG}224$).

2 Dirac materials

In Ref. [28], we used the symmetry-indicators [31, 32] to perform a comprehensive database search for TMs and thousands of TMs were theoretically predicted. By the symmetry-indicator method [32], those materials with band crossings are classified into two subcases: one owning band crossing at high symmetry point while the other owning band crossing lying in high symmetry line or plane [32]. In Refs. [32] and [28], we highlight $MgBi_2O_6$ (space group 136) and OPd (space group 131) as good DSMs, respectively and their DPs are both protected by C_{4v} symmetry. Out of the abundant TMs [28], here we select 8 nearly ideal DSMs with band crossing points near the Fermi level and relatively clean Fermi surfaces. They own Dirac point (DP) either at high symmetry point protected by non-symmorphic symmetry [8, 32] or lying in high symmetry line by band inversion mechanism [9, 10, 32]. They are presented in Table 1, where the positions of the DPs in the Brillouin zone (BZ) are also given. These DSMs crystallize in different space groups ($\mathcal{SG}s$), and own 5 different crystal systems: orthorhombic ($\mathcal{SG}63$), tetragonal ($\mathcal{SG}139$), trigonal ($\mathcal{SG}s166, 167$), hexagonal ($\mathcal{SG}s176, 194$) and cubic ($\mathcal{SG}s223, 224$) lattices. In the following, we will describe their electronic structures for each crystal system and describe the positions of the Dirac band crossings for these DSMs. The detailed symmetry mechanism for these DPs and effective low energy models are left in Section 3.

2.1 Cubic lattice

Firstly we display two cubic and nearly perfect DSMs: Pd_3SrO_4 ($\mathcal{SG}223$) [33] and Ag_2O ($\mathcal{SG}224$) [34]. Their point groups are both O_h and both materials crystallize in the primite cubic lattice. Although there are fruitful spatial symmetries, by a systematic check for all the high symmetry lines or planes which own two or two more different irreducible representations (irreps) [35], it is found that these two materials only have DPs lying in the Γ–X line near the Fermi level and protected by C_{4v} group [35]. Their plots of electronic band and density of states are shown in Figs. 1 and 2, respectively. It is worth mentioning that for Ag_2O ($\mathcal{SG}224$), the Fermi level threads the DP thus the density of states vanishes at the Fermi level as shown in Fig. 1(b). Note that near the Fermi level, the density of states is found to be parabolic in energy consistent with the Dirac cone dispersion, as shown in the inset of Fig. 1(b). The DP in Pd_3SrO_4 ($\mathcal{SG}223$) is very near the Fermi level (around 55 meV below). Furthermore these two oxides are probable to be quite stable in the air

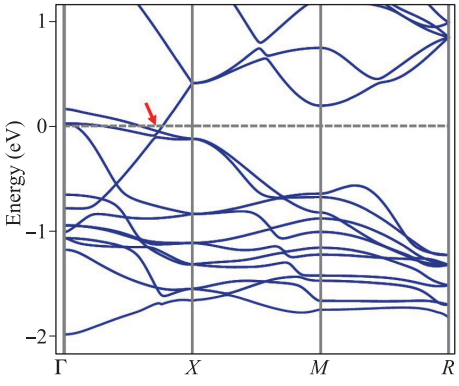

Fig. 2 The electronic band structure for Pd_3SrO_4 ($\mathcal{SG}223$) and the red arrow indicates one DP lying in the high symmetry line Γ–X.

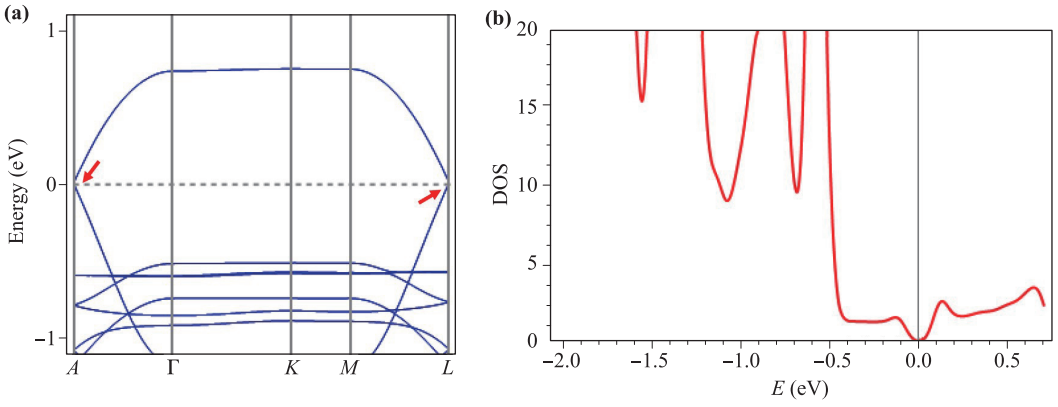

Fig. 3 **(a)** The electronic band structure for $AgCd_3F_{20}Hf_3$ ($\mathcal{SG}176$) and the red arrow indicates one DP at the high symmetry point A. **(b)** The density of states for $AgCd_3F_{20}Hf_3$ ($\mathcal{SG}176$).

and non-toxic, suitable for applications. As a binary compound, Ag_2O seems to be very easy to synthesize, and deserves to be studied in more detail in future.

2.2 Hexagonal lattice

Next we consider the hexagonal lattice, for which the two good DSMs are $AgHf_3Cd_3F_{20}$ ($\mathcal{SG}176$) [36] and Na_2MgSn ($\mathcal{SG}194$) [37, 38]. The former DSM has perfect Fermi surface whose Fermi level exactly threads the DPs which are just the A and L points of the BZ as seen in Fig. 3(a) and has a vanishing density of states at the Fermi level as shown in Fig. 3(b). Such band crossings which occur at high symmetry points can be directly seen from the symmetry indicators [32]. Although the point group of A point is D_{6h}, however, owing to the nonsymmorphic 6-fold screw operation, A has two different 4D irreps. For Na_2MgSn ($\mathcal{SG}194$) (seen Fig. 4), the Dirac band touching (10 meV above the Fermi level) arises from the band inversion between two 2-fold degenerate bands with two different irreps in the high symmetry line Γ–A. This line has symmetries, generated by c_6 and σ_{d1}, whose little group contains 3 different 2D irreps in total. The first principles calculated density of states at the Fermi level is small. Besides, it is worth pointing out that the Fermi level can be tuned to the nearly flat band as shown in Fig. 4 through doping. This could induce electronic instability even under small perturbations, which is a very interesting property to study.

2.3 Orthorhombic lattice

In orthorhombic lattice, we find the nearly ideal DSM named by $K_3Pt_2O_4$ [39] which crystallizes in $\mathcal{SG}63$. The point group of $\mathcal{SG}63$ is D_{2h} and as shown in the irrep character table [35], almost all the high symmetry lines for this $\mathcal{SG}$ contain only one irrep (considering the effect of $\mathcal{T}$). In fact, for $K_3Pt_2O_4$, through checking all the high symmetry lines and points, we find that near the Fermi level, the bands cross only at the high symmetry points Z, T, R. In fact, of all the high symmetry points, only Z, T, R points can host 4D irrep (the DP must be 4-fold generate). Note that R point almost lines with the Fermi level. As shown in the electronic band structure plot in Fig. 5, it is obvious to see that the Dirac band crossings happen in these high symmetry points and are very near to the Fermi level even

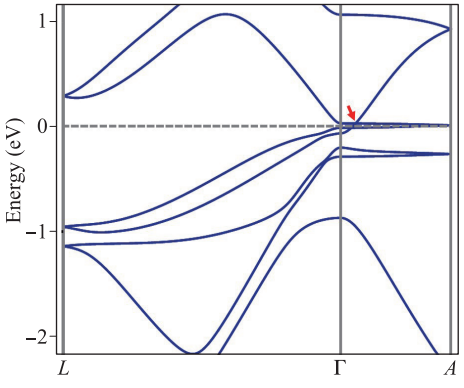

Fig. 4 The electronic band structure for Na_2MgSn ($\mathcal{SG}194$) and the red arrow indicates one DP lying in the high symmetry line Γ–A.

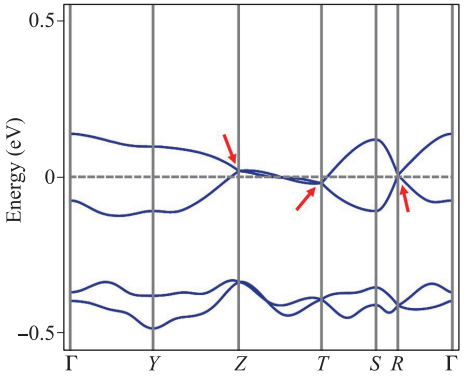

Fig. 5 The electronic band structure for $K_3Pt_2O_4$ ($\mathcal{SG}63$) and the red arrows indicate three DPs at the high symmetry points Z, T, R.

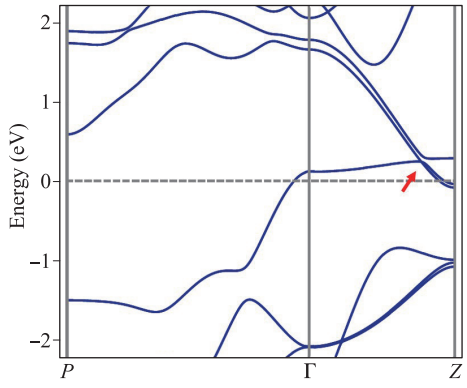

Fig. 6 The electronic band structure for Al_3Nb ($\mathcal{SG}139$) and the red arrow indicates one DP lying in the high symmetry line Γ–Z.

the density of states in the Fermi level is relatively small. As an oxide, this material is probably quite stable in the air and also is promising to be non-toxic.

2.4 Tetragonal lattice

The good DSM in $\mathcal{SG}139$ we find is Al_3Nb [40], whose electronic band structure is shown in Fig. 6. Directly according to the symmetry indicator of this material, it is found that no band crossings at high symmetry points occur near the Fermi level [28, 32]. In $\mathcal{SG}139$, only two (inequivalent) high symmetry lines can host two 2D irreps: Λ and V, while the rest high symmetry lines only have one 2D irrep [35]. The DP is found to be 0.25 meV above the Fermi level and located in the high symmetry line Γ–Z after exhaustive check of these two high symmetry lines. The density of states at the Fermi level is found to be small. As shown in Section 3, the low-energy model always allows linear order term in the $\boldsymbol{k}\cdot\boldsymbol{p}$ Hamiltonian.

2.5 Trigonal lattice

In the trigonal lattice, we selected $NaZn_4As_3$ ($\mathcal{SG}166$) [41] and Cs_8Ga_{11} ($\mathcal{SG}167$) [42] as good DSMs to analyse. They correspond to two aforementioned cases of Dirac band touchings, i.e., lying in high symmetry line and being pinned down at high symmetry points, respectively. As shown in Fig. 7(a) for the electronic energy band of $NaZn_4As_3$ ($\mathcal{SG}166$), the DP is located at high symmetry line Γ–Z. This high symmetry line owns the little group whose generators are c_3 and σ_{d1} [35]. It can host three irreps, whose dimensions are $2, 1, 1$, respectively, of which the last two are related by the joint operation of time-reversal and inversion symmetries [35]. As shown in the plot of density of states in Fig. 7(b), the density of states at the Fermi level is vanishing making this material an ideal DSM candidate.

While for Cs_8Ga_{11} ($\mathcal{SG}167$) shown in Fig. 8, the DPs are located at L and Z high symmetry points. As a matter of fact, by the irrep charcater table [35], we find that only two high symmetry points, L and Z can host 4D irreps. For L, there is only one 4D irrep while for Z point there is two different 4D irreps (it has one more 3-fold rotation symmetry than L point). Note that L point is nearly threaded by the Fermi level. The band plot (Fig. 8) indicates that the DPs are very close to the Fermi level although the density of states at the Fermi level is not very small since there are several bands crossing the Fermi level. Thus this material is also very interesting for realistic applications.

3 Derivation of $k\cdot p$ effective models

3.1 Dirac point in high symmetry line

In this and next section, we show the derivations of low energy models for all the above DSMs around the band crossings indicated in the band plots. To express the low energy model, we use the 16 Γ matrices chosen as identity matrix (I), 5 Dirac matrices Γ^i and their 10 commutators $\Gamma^{ij} = [\Gamma^i, \Gamma^j]/(2\mathrm{i})$. The 5 Dirac matrices are $\Gamma^{(1,2,3,4,5)} = \{\sigma_x\otimes\sigma_0, \sigma_z\otimes\sigma_0, \sigma_y\otimes\sigma_x, \sigma_y\otimes\sigma_y, \sigma_y\otimes\sigma_z\}$ where σ_0 is 2×2 identity matrix and $\sigma_x, \sigma_y, \sigma_z$ are Pauli matrices. The Dirac band crossings are classified into two kinds: one lying in a high symmetry line [9, 10, 32] and

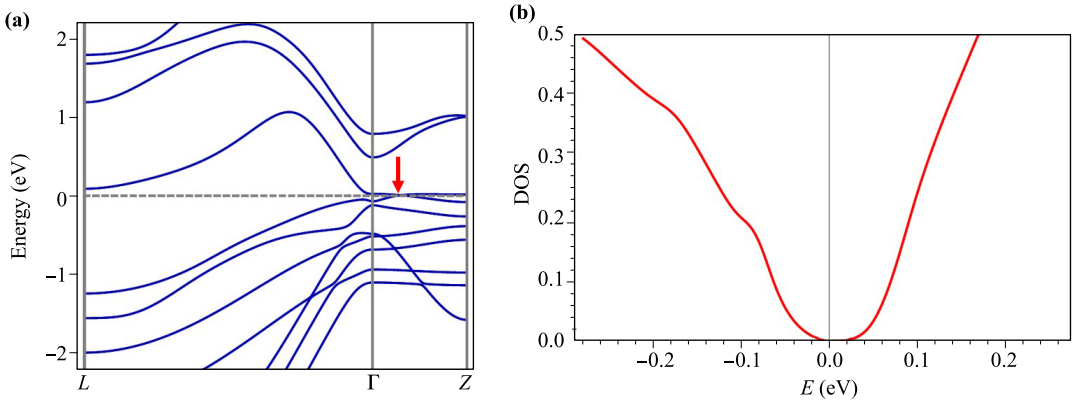

Fig. 7 **(a)** The electronic band structure for $NaZn_4As_3$ ($\mathcal{SG}166$) and the red arrow indicates one DP lying in the high symmetry line Γ–Z. **(b)** The density of states for $NaZn_4As_3$ ($\mathcal{SG}166$).

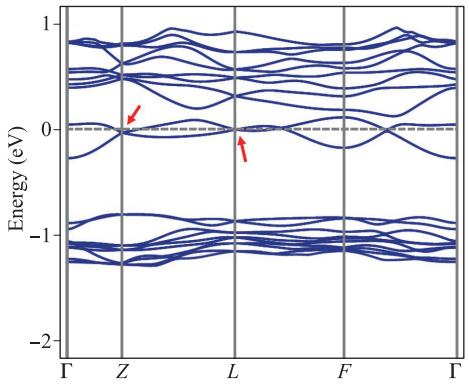

Fig. 8 The electronic band structure for Cs_8Ga_{11} ($\mathcal{SG}167$) and the red arrows indicate two DP at the high symmetry points L and Z.

the other pinned down at high symmetry point [8, 32]. In this subsection, we first discuss the former case.

For Al_3Nb ($\mathcal{SG}139$), the DP in the high symmetry line Γ–Z is found to be at $\boldsymbol{k}_{DP} = (0, 0, 0.3128\,\text{Å}^{-1})$. It is protected by C_{4v} symmetry and originated from band inversion between two doubly-degenerate bands which belong to two different irreps (note that C_{4v} only has two different 2D irreps when time reversal symmetry is considered). The low energy $\boldsymbol{k}\cdot\boldsymbol{p}$ model near the DP is found to be $v_0q_zI + v_1q_x\Gamma^1 + v_1q_y\Gamma^5 + v_3q_z\Gamma^2$ where $(q_x, q_y, q_z) = \boldsymbol{q} - \boldsymbol{k}_{DP}$ is the displacement away from the DP $\boldsymbol{k}_{DP}$ and v_0, v_1, v_3 are parameters.

Note that the denoted DPs in Ag_2O ($\mathcal{SG}224$) and Pd_3SrO_4 ($\mathcal{SG}223$) are located in Γ–X line, but due to the O_h symmetry, C_{4y} can relate these DPs with another ones located in Γ–Z line. The low energy model around the DP in Γ–Z line owns the same form as that of Al_3Nb ($\mathcal{SG}139$) in the above since they both have C_{4v} symmetry and the orientation of 4-fold axis is along z-axis. Their DPs' coordinates are $(0, 0, 0.1240\,\text{Å}^{-1})$ and $(0, 0, 0.4044\,\text{Å}^{-1})$, respectively.

For As_3NaZn ($\mathcal{SG}166$), the DP is located in the high symmetry line Γ–Z protected by C_{3v} symmetry whose coordinate is $(0, 0, 0.02868\,\text{Å}^{-1})$. It is due to a band crossing between the doubly-degenerate bands belongs to the only two different irreps. The low energy near this DP is found to be $v_0q_zI + (v_1q_x - v_2q_y)\Gamma^1 + (v_2q_x + v_1q_y)\Gamma^5 + \frac{(q_x-\sqrt{3}q_y)v_1+(\sqrt{3}q_x+q_y)v_2}{2}\Gamma^3 + \frac{(\sqrt{3}q_x+q_y)v_1+(-q_x+\sqrt{3}q_y)v_2}{2}\Gamma^4 + v_3q_z\Gamma^2$ where v_0, v_1, v_2, v_3 are parameters.

For Na_2MgSn ($\mathcal{SG}194$), the DP ($(0, 0, 0.01867\,\text{Å}^{-1})$) is located in Γ–A whose point group is C_{6v}, which has three 2D irreps. For this material, the DP is the band crossing between two doubly-degenerate bands with two different irreps, whose eigenvalues of C_{6v} are (i, −i) and $(e^{i\frac{\pi}{6}}, e^{-i\frac{\pi}{6}})$ where each parenthesis denotes a 2D irrep. We finally find the low energy can be written as: $v_0q_zI + v_3q_z\Gamma^2 + v_1(q_x + \sqrt{3}q_y)\Gamma^5 + v_1(\sqrt{3}q_x - q_y)\Gamma^1$ where v_0, v_1, v_3 are parameters.

It is interesting to note that when only one of the inversion and σ_v symmetries is broken, the DPs would still exist for C_n symmetry cases where $n = 4$ and 6 while for $n = 3$, the DP would evolve into two triply-degenerate band crossings. When they are both broken, four (except that for $n = 3$, the number may be 3 or 4) Weyl points would occur from the DP which are protected by just c_n rotation symmetry.

3.2 Dirac point at high symmetry point

For the rest materials, the DPs are located at high symmetry points. Next we analyse the symmetry protection mechanisms for these DPs case by case. First for $K_3Pt_2O_4$, as Z and T points have exactly the same little group [35], they are first analysed together. The generators of the little group are screw operation $\tilde{c}_{2z} = (-x, -y, z + \frac{1}{2})$, rotation $c_{2x} = (x, -y, -z)$ and inversion $P = (-x, -y, -z)$ where we use the Jones' faithful representation [35] under the conventional basis vectors for orthorhombic lattice. Since $\{\tilde{c}_{2z}, P\} = 0$ for Z and T points, thus $\tilde{c}_{2z}$ could relate two states with opposite parities, i.e., if we choose $|+\rangle$ as the common eigensate of P and Hamiltonian with even parity, $\tilde{c}_{2z}|+\rangle$ would have an odd parity. Besides, c_{2x} preserves the parity, thus the eigenstate of Hamiltonian can be labelled additionally by the eigenvalue of c_{2x}, i.e., $\pm$i. Hence, considering $\mathcal{T}$, $|+, \text{i}\rangle, \tilde{c}_{2z}|+, \text{i}\rangle, \mathcal{T}|+, \text{i}\rangle, \mathcal{T}\tilde{c}_{2z}|+, \text{i}\rangle$ constitute the basis for the only 4D irrep. The above-mentioned operators can be represented by 4×4 matrices in the basis easily. Thus the low energy Hamiltonian is found to $v_3q_z\Gamma^{13} + v_2q_y\Gamma^{35} + (m_1q_x^2 + m_2q_y^2 + m_3q_z^3)I + v_{23}q_yq_z\Gamma^{34}$ where $v_2, v_3, m_1, m_2, m_3, v_{23}$ are parameters. On the contrary, for R point, different from Z and T points, c_{2x} is not the symmetry operation, thus the basis for the only 4D irrep is $|+\rangle, \tilde{c}_{2z}|+\rangle, \mathcal{T}|+\rangle, \mathcal{T}\tilde{c}_{2z}|+\rangle$, and the low energy Hamiltonian in this basis is found to be: $(v_3q_z)\Gamma^3 + (v_3'q_z)\Gamma^{13} + (v_3''q_z)\Gamma^{23} + (v_1q_x + v_2q_y)\Gamma^{35}$ where $v_3, v_3', v_3'', v_1, v_2$ are parameters.

For Cs_8Ga_{11}, firstly we analyse the Z point which is subject to $c_3 = (z, x, y)$, $\tilde{c'}_{21} = (-x + \frac{1}{2}, -z + \frac{1}{2}, -y + \frac{1}{2})$ and $P = (-x, -y, -z)$ under the trigonal lattice basis vectors. Note that $[c_3, P] = 0$, thus we can choose the eigenvalues of P and c_3 to label the energy level: $|+, -1\rangle, |+, e^{i\frac{\pi}{3}}\rangle, |+, e^{-i\frac{\pi}{3}}\rangle$ where for each ket vector, $+$ represent even parity and the other number is the eigenvalue of c_3. $\tilde{c'}_{21}$ operating one these three states would obtain another three states all with odd parity. Furthermore, $\tilde{c'}_{21}|+, 1\rangle$ is also the eigenstate of c_3 whose eigenvalue is 1, while $\tilde{c'}_{21}|+, e^{\pm i\frac{\pi}{3}}\rangle$ is the eigenstate of c_3 with eigenvalue being $e^{\mp i\frac{\pi}{3}}$. Operating $\mathcal{T}$ on the above states, we find two 4D irreps: for one 4D irrep, the basis can be chosen as $|+, -1\rangle, \tilde{c'}_{21}|+, -1\rangle, \mathcal{T}|+, -1\rangle, \mathcal{T}\tilde{c'}_{21}|+, -1\rangle$ while the basis for the other 4D irrep can be chosen as $|+, e^{i\frac{\pi}{3}}\rangle, \tilde{c'}_{21}|+, e^{i\frac{\pi}{3}}\rangle, \mathcal{T}|+, e^{i\frac{\pi}{3}}\rangle, \mathcal{T}\tilde{c'}_{21}|+, e^{i\frac{\pi}{3}}\rangle$. In this material, the DP corresponds to the second basis from the first principles calculations, and then the low energy model is found to be $v_3q_z\Gamma^3 + v_1(q_x\Gamma^{35} + q_y\Gamma^{13}) + v_3'q_z\Gamma^{23}$ where v_1, v_3, v_3' are parameters and note that the 2-fold axis for

$\tilde{c}'_{21}$ is set to be along our $x-$axis for the $\boldsymbol{k}\cdot\boldsymbol{p}$ Hamiltonian. For L point, the symmetry operations only contain $\tilde{c}'_{22} = (-z+\frac{1}{2}, -y+\frac{1}{2}, -x+\frac{1}{2})$ and P. Thus the basis for the only 4D irrep can be chose as $|+\rangle, \tilde{c}'_{22}|+\rangle, \mathcal{T}|+\rangle, \mathcal{T}\tilde{c}'_{22}|+\rangle$ under which the low energy Hamiltonian is $(v_1q_y+v_2q_z)\Gamma^3 + (v_3q_y + v_4q_z)\Gamma^{13} + (v_5q_y + v_6q_z)\Gamma^{23} + v_7q_x\Gamma^{35}$ where $v_i's$ are all parameters and note that the 2-fold axis for c'_{22} is set to be along our $x-$axis for the $\boldsymbol{k}\cdot\boldsymbol{p}$ Hamiltonian.

Finally we analyse $AgCd_3F_{20}Hf_3$ whose DP is just the A high symmetry point. It has $\tilde{c}_6 = (x-y, x, z+\frac{1}{2})$ and $P = (-x, -y, -z)$ symmetries. As $\{\tilde{c}_6, P\} = 0$ and $[\tilde{c}_6^2, P] = 0$, thus we can first label the energy level by parity and the eigenvalue of $\tilde{c}_6^2$: $|+,1\rangle, |+, e^{i\frac{2\pi}{3}}\rangle, |+, e^{-i\frac{2\pi}{3}}\rangle$. $\tilde{c}_6$ would reverse their parity while preserve the eigenvalue the $\tilde{c}_6^2$. Thus there are two 4D irreps for which the bases can be chosen as $|+,1\rangle, \tilde{c}_6|+,1\rangle, \mathcal{T}|+,1\rangle, \mathcal{T}\tilde{c}_6|+,1\rangle$ and $|+, e^{i\frac{2\pi}{3}}\rangle, \tilde{c}_6|+, e^{i\frac{2\pi}{3}}\rangle, \mathcal{T}|+, e^{i\frac{2\pi}{3}}\rangle, \mathcal{T}\tilde{c}_6|+, e^{i\frac{2\pi}{3}}\rangle$, respectively. The band structure calculation shows that the DP corresponds to the second situation, and the low energy model is found to be $v_3q_z(\Gamma_{13} + \sqrt{3}\Gamma_{35}) + (m_3q_z^2 + m_1q_x^2 + m_1q_y^2)I$ where m_1, m_2, m_3 and v_3 are parameters. For L point, the generators of its symmetry are $P = (-x, -y, -z)$ and $\sigma_h = (x, y, -z+\frac{1}{2})$. As $\{P, \sigma_h\} = 0$, we can obtain the basis for only one 4D irrep as: $|+\rangle, \sigma_h|+\rangle, \mathcal{T}|+\rangle, \mathcal{T}\sigma_h|+\rangle$ where $+$ denotes even parity. The $\boldsymbol{k}\cdot\boldsymbol{p}$ model is found to be: $(v_1q_x + v_2q_y)\Gamma^3 + v_3q_z\Gamma^{13} + (v'_1q_x + v'_2q_y)\Gamma^{23} + (v''_1q_x + v''_2q_y)\Gamma^{35}$ where $v_1, v_2, v'_1, v'_2, v''_1, v''_2$ and v_3 are all parameters.

4 Conclusion

In conclusion, we have presented $\boldsymbol{k}\cdot\boldsymbol{p}$ model analyses for some ideal or nearly ideal Dirac semimetals. These $\boldsymbol{k}\cdot\boldsymbol{p}$ models are sufficient to show that the low energy physics in these system is exactly the Dirac one. Besides, these $\boldsymbol{k}\cdot\boldsymbol{p}$ Hamiltonians can serve as the starting point for further calculations such as electronic transport properties, electron–electron correlation, etc. Finally, the Dirac materials highlighted in this work deserve further experimental studies for physical properties related with the nontrivial band topology, and some of them may find applications in realistic electronics.

5 Method

The electronic band structure calculations have been carried out using the full potential linearized augmented plane-wave method as implemented in the WIEN2K package [43]. The generalized gradient approximation (GGA) with Perdew–Burke–Ernzerhof (PBE) [44] realization was adopted for the exchange-correlation functional.

Acknowledgements This work was supported by the National Natural Science Foundation of China (Nos. 11525417, 11834006, 51721001, and 11790311) and the National Key R&D Program of China (Nos. 2018YFA0305704 and 2017YFA0303203).

References

1. K. Klitzing, G. Dorda, and M. Pepper, New method for high-accuracy determination of the fine-structure constant based on quantized Hall resistance, *Phys. Rev. Lett.* 45(6), 494 (1980)
2. D. J. Thouless, M. Kohmoto, M. P. Nightingale, and M. den Nijs, Quantized Hall conductance in a two-dimensional periodic potential, *Phys. Rev. Lett.* 49(6), 405 (1982)
3. M. Z. Hasan and C. L. Kane, Colloquium: Topological insulators, *Rev. Mod. Phys.* 82(4), 3045 (2010)
4. X. L. Qi and S. C. Zhang, Topological insulators and superconductors, *Rev. Mod. Phys.* 83(4), 1057 (2011)
5. Y. Ando and L. Fu, Topological crystalline insulators and topological superconductors: From concepts to materials, *Annu. Rev. Condens. Matter Phys.* 6(1), 361 (2015)
6. N. P. Armitage, E. J. Mele, and A. Vishwanath, Weyl and Dirac semimetals in three-dimensional solids, *Rev. Mod. Phys.* 90(1), 015001 (2018)
7. T. O. Wehling, A. M. Black-Schaffer, and A. V. Balatsky, Dirac materials, *Adv. Phys.* 63(1), 1 (2014)
8. S. M. Young, S. Zaheer, J. C. Y. Teo, C. L. Kane, E. J. Mele, and A. M. Rappe, Dirac semimetal in three dimensions, *Phys. Rev. Lett.* 108(14), 140405 (2012)
9. Z. Wang, Y. Sun, X.Q. Chen, C. Franchini, G. Xu, H. Weng, X. Dai, and Z. Fang, Dirac semimetal and topological phase transitions in A_3Bi (A = Na, K, Rb), *Phys. Rev. B* 85(19), 195320 (2012)
10. Z. Wang, H. Weng, Q. Wu, X. Dai, and Z. Fang, Three-dimensional Dirac semimetal and quantum transport in Cd_3As_2, *Phys. Rev. B* 88(12), 125427 (2013)
11. Z. K. Liu, B. Zhou, Y. Zhang, Z. J. Wang, H. M. Weng, D. Prabhakaran, S. K. Mo, Z. X. Shen, Z. Fang, X. Dai, Z. Hussain, and Y. L. Chen, Discovery of a three-dimensional topological Dirac semimetal, Na_3Bi, *Science* 343(6173), 864 (2014)
12. Z. K. Liu, J. Jiang, B. Zhou , Z. J. Wang, Y. Zhang, H. M. Weng, D. Prabhakaran, S.-K. Mo, H. Peng, P. Dudin6 , T. Kim, M. Hoesch, Z. Fang, X. Dai, Z. X. Shen, D. L. Feng, Z. Hussain, and Y. L. Chen, A stable three-dimensional topological Dirac semimetal Cd_3As_2, *Nat. Mater.* 13, 677C681 (2014)
13. B. J. Yang and N. Nagaosa, Classification of stable three-dimensional Dirac semimetals with nontrivial topology, *Nat. Commun.* 5(1), 4898 (2014)
14. M. I. Katsnelson, K. S. Novoselov, and A. K. Geim, Chiral tunnelling and the Klein paradox in graphene, *Nat. Phys.* 2(9), 620 (2006)
15. M. Yan, H. Huang, K. Zhang, E. Wang, W. Yao, K. Deng, G. Wan, H. Zhang, M. Arita, H. Yang, Z. Sun, H. Yao, Y. Wu, S. Fan, W. Duan, and S. Zhou, Lorentz-violating type-II Dirac fermions in transition metal dichalcogenide $PtTe_2$, *Nat. Commun.* 8(1), 257 (2017)

16. H. J. Noh, J. Jeong, E. J. Cho, K. Kim, B. I. Min, and B. G. Park, Experimental realization of type-II Dirac fermions in a $PdTe_2$ superconductor, *Phys. Rev. Lett.* 119(1), 016401 (2017)
17. F. Fei, X. Bo, R. Wang, B. Wu, J. Jiang, D. Fu, M. Gao, H. Zheng, Y. Chen, X. Wang, H. Bu, F. Song, X. Wan, B. Wang, and G. Wang, Nontrivial Berry phase and type-II Dirac transport in the layered material $PdTe_2$, *Phys. Rev. B* 96(4), 041201 (2017)
18. Q. D. Gibson, L. M. Schoop, L. Muechler, L. S. Xie, M. Hirschberger, N. P. Ong, R. Car, and R. J. Cava, Three-dimensional Dirac semimetals: Design principles and predictions of new materials, *Phys. Rev. B* 91(20), 205128 (2015)
19. Q. S. Wu, C. Piveteau, Z. Song, and O. V. Yazyev, $MgTa_2N_3$: A reference Dirac semimetal, *Phys. Rev. B* 98, 081115(R) (2018)
20. W. D. Cao, P. Z. Tang, S.-C. Zhang, W. H. Duan, and A. Rubio, Stable Dirac semimetal in the allotropes of group-IV elements, *Phys. Rev. B* 93, 241117(R) (2016)
21. X. Zhang, Q. Liu, Q. Xu, X. Dai, and A. Zunger, Topological insulators versus topological Dirac semimetals in honeycomb compounds, *J. Am. Chem. Soc.* 140(42), 13687 (2018)
22. X. L. Sheng, Z. Wang, R. Yu, H. Weng, Z. Fang, and X. Dai, Topological insulator to Dirac semimetal transition driven by sign change of spin–orbit coupling in thallium nitride, *Phys. Rev. B* 90(24), 245308 (2014)
23. Y. Du, B. Wan, D. Wang, L. Sheng, C.G. Duan, and X. Wan, Dirac and Weyl semimetal in $XYBi$ (X = Ba, Eu; Y = Cu, Ag and Au), *Sci. Rep.* 5(1), 14423 (2015)
24. Y. P. Du, F. Tang, D. Wang, L. Sheng, E. J. Kan, C.-G. Duan, S. Y. Savrasov, and X. G. Wan, CaTe: A new topological node-line and Dirac semimetal, *npj Quant. Mater.* 2, 3 (2017)
25. R. Chen, H. C. Po, J. B. Neaton, and A. Vishwanath, Topological materials discovery using electron filling constraints, *Nat. Phys.* 14(1), 55 (2018)
26. T. Zhang, Y. Jiang, Z. Song, H. Huang, Y. He, Z. Fang, H. Weng, and C. Fang, Catalogue of topological electronic materials, *Nature* 566(7745), 475 (2019)
27. M. G. Vergniory, L. Elcoro, C. Felser, N. Regnault, B. A. Bernevig, and Z. Wang, A complete catalogue of high-quality topological materials, *Nature* 566(7745), 480 (2019)
28. F. Tang, H. C. Po, A. Vishwanath, and X. Wan, Comprehensive search for topological materials using symmetry indicators, *Nature* 566(7745), 486 (2019)
29. J. Xiong, S. K. Kushwaha, T. Liang, J. W. Krizan, M. Hirschberger, W. Wang, R. J. Cava, and N. P. Ong, Evidence for the chiral anomaly in the Dirac semimetal Na_3Bi, *Science* 350(6259), 413 (2015)
30. M. Neupane, S. Y. Xu, R. Sankar, N. Alidoust, G. Bian, C. Liu, I. Belopolski, T. R. Chang, H. T. Jeng, H. Lin, A. Bansil, F. Chou, and M. Z. Hasan, Observation of a three-dimensional topological Dirac semimetal phase in high-mobility Cd_3As_2, *Nat. Commun.* 5(1), 3786 (2014)
31. H. C. Po, A. Vishwanath, and H. Watanabe, Symmetry-based indicators of band topology in the 230 space groups, *Nat. Commun.* 8(1), 50 (2017)
32. F. Tang, H. C. Po, A. Vishwanath, and X. Wan, Efficient topological materials discovery using symmetry indicators, *Nat. Phys.* 15, 470 (2019)
33. O. Muller and R. Roy, Synthesis and crystal chemistry of some new complex palladium oxides, *Adv. Chem. Ser.* 98, 28 (1971)
34. P. Norby, R. E. Dinnebier, and A. N. Fitch, Decomposition of silver carbonate: the crystal structure of two high-temperature modifications of Ag_2CO_3, *Inorg. Chem.* 41(14), 3628 (2002)
35. C. J. Bradley and A. P. Cracknell, The Mathematical Theory of Symmetry in Solids, Oxford: Claredon Press, 1972
36. O. Graudejus and B. G. Mueller, Ag^{2+} in trigonalbipyramidaler Umgebung: Neue Fluoride mit zweiwertigem Silber: Ag M(II)$_3$ M(IV)$_3$ F$_{20}$ (M(II) = Cd, Ca, Hg; M(IV) = Zr, Hf), Zeitschrift fuer Anorganische und Allgemeine Chemie (1950) (DE) 622, 1549–1556 (1996)
37. T. Yamada, V. L. Deringer, R. Dronskowski, and H. Yamane, Synthesis, crystal structure, chemical bonding, and physical properties of the ternary Na/Mg stannide, Na_2MgSn, *Inorg. Chem.* 51(8), 4810 (2012)
38. B. Peng, C. M. Yue, H.Zhang, Z. Fang, and H. M.Weng, Predicting Dirac semimetals based on sodium ternary compounds, *npj Comput. Mater.* 4, 68 (2018)
39. H. Zentgraf, K. Claes, and R. Hoppe, Oxide eines neuen Formeltyps: Zur Kenntnis von $K_3Ni_2O_4$ und $K_3Pt_2O_4$, Zeitschrift fuer Anorganische und Allgemeine Chemie (1950) (DE) 462, 92–105 (1980)
40. Z. Nong, J. Zhu, X. Yang, Y. Cao, Z. Lai, and Y. Liu, The mechanical, thermodynamic and electronic properties of Al_3Nb with DO_{22} structure: A first-principles study, *Physica B* 407(17), 3555 (2012)
41. H. He, C. Tyson, and S. Bobev, Eight-coordinated arsenic in the Zintl phases $RbCd_4As_3$ and $RbZn_4As_3$: Synthesis and structural characterization, *Inorg. Chem.* 50(17), 8375 (2011)
42. R. W. Henning and J. D. Corbett, Cs_8Ga_{11}, a new isolated cluster in a binary gallium compound: A family of valence analogues $A_8Tr_{11}X$: A = Cs, Rb; Tr = Ga, In, Tl; X = Cl, Br, I, *Inorg. Chem.* 36(26), 6045 (1997)
43. P. Blaha, K. Schwarz, G. Madsen, D. Kvasicka, and J. Luitz, WIEN2k: An Augmented Plane Wave Plus Local Orbitals Program for Calculating Crystal Properties, 2001
44. J. P. Perdew, K. Burke, and M. Ernzerhof, Generalized gradient approximation made simple, *Phys. Rev. Lett.* 77(18), 3865(1996)